Catena 166 (2018) 78–88

Contents lists available at ScienceDirect

Catena

journal homepage: www.elsevier.com/locate/catena

Effects of human activities on pedogenesis and iron dynamics in paddy soils developed on Quaternary red clays

Lai-Ming Huang[a,b,c,d], Min-An Shao[a,c,d,*], Fang Huang[e], Gan-Lin Zhang[b,c,**]

[a] Key Laboratory of Ecosystem Network Observation and Modeling, Institute of Geographic Sciences and Natural Resources Research, Chinese Academy of Sciences, Beijing 100101, China
[b] State Key Laboratory of Soil and Sustainable Agriculture, Institute of Soil Science, Chinese Academy of Sciences, Nanjing 210008, China
[c] College of Resources and Environment, University of Chinese Academy of Sciences, Beijing 100049, China
[d] State Key Laboratory of Soil Erosion and Dryland Farming on the Loess Plateau, Institute of Soil and Water Conservation, CAS & MWR, College of Natural Resources and Environment, Northwest A & F University, China
[e] School of Earth and Space Sciences, University of Science and Technology of China, Heifei 230026, China

ARTICLE INFO

Keywords:
Anthropedogenesis
Soil chronosequence
Fe oxides
δ^{56}Fe
Temporal changes

ABSTRACT

A paddy soil chronosequence consisting of four profiles derived from Quaternary red clay (QRC) in Southern China with cultivation history from 0 to 300 years was studied to understand the underlying mechanisms and processes controlling the centennial scale Fe evolution during anthropedogenesis. We evaluated the chronosequencial changes in depth distribution of Fe oxides and Fe isotopic compositions. Results showed that paddy soil development on QRC over a centennial time scale caused increasing profile differentiation of Fe oxides and measurable Fe isotope fractionation. Total Fe and oxide bound Fe as well as the maximum Fe illuviation depth decreased as paddy soils age, leading to significant differences in morphological properties between paddy and non-paddy soils with the same parent material. Selective extractions showed that the weakly-bound, oxide-bound and silicate bound Fe corresponded to 4–18%, 49–81%, and 11–40% of the total Fe, respectively, and these proportions varied with both time and depth due to the redox-related Fe transformation and redistribution. δ^{56}Fe values in the studied paddy soil chronosequence ranged from 0.05‰ to 0.26‰ and exhibited a strong negative correlation with the logarithm of total Fe concentrations, suggesting mass-dependent Fe isotope fractionation occurred as a result of the preferential removal of lighter Fe isotopes during Fe leaching loss under the predominant reducing conditions. However, the Fe isotopic ratio of a specific paddy soil horizon was a result of a complex interaction of different processes, which were summarized and interpreted in our proposed conceptual model of Fe evolution in terraced paddy soils. Further investigations of Fe isotope signatures in the soil-plant-water system with a combination of laboratory simulation and prediction of Fe isotope fractionation under different pedogenic processes are needed to evaluate the relative contribution of multiple processes to Fe isotope fractionation during anthropedogenesis of paddy soils.

1. Introduction

Quaternary red clay (QRC) formed by chemical weathering under wet tropical and subtropical conditions is widely distributed in Southern China (Li, 1983) as well as in other countries around the world (Muggler et al., 2001). It is characterized by the red color, strong acidity, clayey structure, and high degree of weathering (Li, 1983; Muggler et al., 2001) due to the coincidence of high temperature and heavy rainfall. As a result, QRC shows substantial leaching of mobile elements (e.g., Ca, Mg, Na, and K), relative enrichment of Fe and Al, and a dominant clay mineral composition of kaolinite (Gong, 1985; He et al., 2008; Hu et al., 2010; Hong et al., 2014). Soils developed on QRC consist of a variety of different Fe phases, such as primary silicate minerals, pedogenic clay minerals, Fe (oxyhydr)oxides with different degrees of crystallinity, as well as in organic complexes. Previous studies have shown that Fe (oxyhydr)oxides undergo significant changes in species, amounts, and stability during the course of soil development, which are caused by chemical weathering, redox reactions, and the

* Correspondence to: M.-A. Shao, Key Laboratory of Ecosystem Network Observation and Modeling, Institute of Geographic Sciences and Natural Resources Research, Chinese Academy of Sciences, Beijing 100101, China.
** Corresponding author at: State Key Laboratory of Soil and Sustainable Agriculture, Institute of Soil Science, Chinese Academy of Sciences, NO. 71 East Beijing Road, Nanjing 210008, China.
E-mail addresses: shaoma@igsnrr.ac.cn (M.-A. Shao), glzhang@issas.ac.cn (G.-L. Zhang).

https://doi.org/10.1016/j.catena.2018.03.019
Received 13 December 2017; Received in revised form 7 March 2018; Accepted 22 March 2018

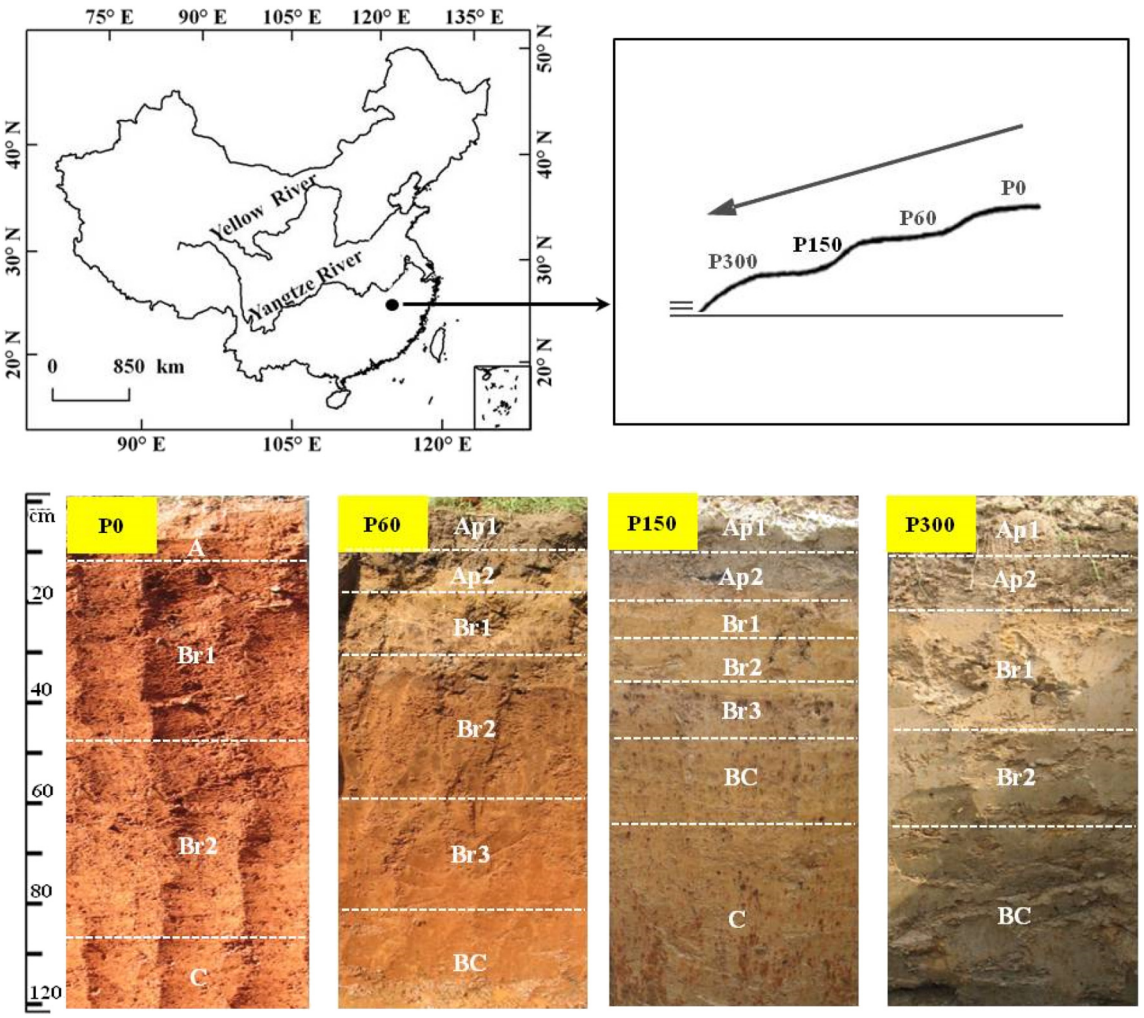

Fig. 1. Location of the study area and sampling sites, and representative soil profiles (P0, P60, P150, and P300) with 0, 60, 150, and 300 years of rice cultivation history.

lattice replacement of other metals with Fe in Fe-bearing minerals (van Breemen and Buurman, 2004; Vodyanitskii, 2010). The ratio of dithionite-citrate-bicarbonate extractable Fe to total Fe generally increases while the ratio of oxalate extractable Fe to total Fe decreases with increasing pedogenic age as indicated by the selective chemical extractions (Torrent et al., 1980; Aniku and Singer, 1990). In addition, the crystallinity of Fe (oxyhydr)oxides and the amount of Al that substitutes Fe in goethite often increase with increasing soil development (Cornell and Schwertmann, 2003). Therefore, the pedogenic Fe mobilization, translocation, and redistribution as well as the associated Fe mineral transformation are key processes in soil formation that influence the morphological and physico-chemical properties of soils (van Breemen and Buurman, 2004; Vodyanitskii, 2010).

The natural pedogenic controls on Fe evolution may be superseded by human activities (Dudal, 2005) that alter the rate and trajectory of net Fe dynamics either directly (e.g., by mineral and/or organic fertilizer additions) or indirectly (e.g., by alternate flooding and draining in rice paddies). For instance, paddy soils originating from QRC are widely distributed in Southern China, and are highly modified by anthropogenic management during paddy cultivation (Huang et al., 2015). The periodic artificial flooding and draining as well as groundwater fluctuations during paddy soil evolution result in significant changes in soil moisture regime and redox conditions with both time and depth, leading to coupled reduction-oxidation and eluviation-illuviation processes of Fe and formation of diagnostic horizons and features in paddy soil profiles (Gong, 1983, 1986; Zhang and Gong, 1993, 2003). The redox changes of Fe in paddy soils are accompanied by the mobilization and translocation of Fe within soil profiles and transport of Fe as well as other redox sensitive elements to water bodies (Li, 1992; Kyuma, 2004). Despite the extensive researches during the past several decades on biogeochemical Fe cycling in paddy soils, the investigations have been limited to inferences from chemical extraction (e.g., Zhang and Gong, 2003), magnetic measurement (e.g., Han and Zhang, 2013; Chen et al., 2015) and mineralogical analysis (e.g., Han et al., 2015). The recent development of multi-collector inductively coupled plasma mass spectrometry (MC-ICP-MS) has drawn growing interests in the study of stable Fe isotopes, and this new tool has been widely used to trace the geochemical and biological cycling of Fe under both natural and experimental conditions (Dauphas et al., 2017).

Fe possesses four stable isotopes, ^{54}Fe, ^{56}Fe, ^{57}Fe, and ^{58}Fe, with natural abundance percentage of 5.84%, 91.75%, 2.12%, and 0.29%, respectively. The isotopic composition of Fe is usually reported as δ^{56}Fe, which is the deviation in parts per mil of the ^{56}Fe/^{54}Fe ratio relative to the IRMM-014 reference standard. δ^{57}Fe is also reported in literature, which is approximately equal to 1.5-fold of δ^{56}Fe (i.e. $\delta^{57}Fe \approx 1.5 \times \delta^{56}Fe$) due to the observed mass-dependent fractionation (Dauphas and Rouxel, 2006). It has been well established that Fe isotopes can be fractionated by kinetic and/or equilibrium effects during both biological and abiological processes (Kappler et al., 2010; Anbar, 2004; Johnson et al., 2004; Matthews et al., 2001; Anbar et al., 2000; Beard et al., 1999). Laboratory studies have shown that both ligand-promoted (Wiederhold et al., 2006; Brantley et al., 2004; Brantley et al.,

2001) and reductive (Crosby et al., 2007, 2005; Beard et al., 1999) dissolution of Fe-bearing minerals result in preferential removal of lighter Fe isotopes, thereby enriching the residual solids in heavier Fe isotopes. In contrast, there is no detectable Fe isotope fractionation during the proton-promoted dissolution (Wiederhold et al., 2006; Skulan et al., 2002). Adsorption processes are known to preferentially sequester the heavier Fe isotope at mineral surfaces (Icopini et al., 2004) and the precipitation of ferric oxides from aqueous solutions also yields isotopically heavy solid phases (Balci et al., 2006). These laboratory-controlled experiments generally focused on a single isolated process, a condition that cannot be extrapolated to the field, but the results have been proved to provide important clues for the interpretation of Fe isotope fractionation mechanisms in natural soil environments.

Fe isotope studies in the worldwide soils have demonstrated measureable Fe isotope fractionation during weathering and soil formation, but the direction and magnitude of Fe isotope fractionation vary markedly among different soil types (Huang et al., 2018b). Paddy soils make up the largest anthropogenic wetlands on earth and thus represent a key component of the Fe geochemical cycle at the Earth's surface. Previous studies have investigated the changing status of Fe oxides (Yu, 1985; Gong, 1986) and Fe isotopes (Garnier et al., 2017) at a given stage of paddy soil evolution through a comparison with the initial parent material. However, little is known about the successive changes of Fe oxides and Fe isotopic composition during paddy soil evolution that is required to identify process rates and thresholds of Fe dynamics.

Soil chronosequence provides a valuable tool for investigating the rates and directions of soil evolution (Huang et al., 2015). In this study, we measured different forms of Fe oxides and stable Fe isotope compositions in a paddy soil chronosequence consisting of four profiles derived from QRC in Southern China with cultivation history ranging from 0 to 300 years (Fig. 1). Our objectives were to (i) investigate the dynamic changes in Fe oxides and Fe isotope compositions during anthropedogenesis of paddy soils on slope uplands; (ii) identify the underlying mechanisms and processes controlling centennial scale Fe evolution; (iii) establish a conceptual model characterizing Fe transfer and redistribution in paddy soils on slope uplands and assess their impacts on Fe isotope fractionation.

2. Materials and methods

2.1. Study area and sampling sites

The study area is located on a slope upland in Jinxian County, Jiangxi Province, South China, between 116°1′–116°32′ E and 28°2′–28°26′ N (Fig. 1). This region belongs to the southern fringe of northern subtropics, which has a mean annual air temperature of 17 °C, with yearly extremes from 5 °C to 40 °C, and a mean annual precipitation of 1587 mm, of which 79% is concentrated in the rice paddy flooding season (April to October). Terraced paddy fields are a common feature in this area. Soils are derived primarily from acid quaternary red clays, which are highly weathered, clay rich and phosphorus deficient (Han and Zhang, 2013; Han et al., 2015; Huang et al., 2013, 2014). Soils at the bottom of slopes were generally the first to be converted to paddy field; as population pressure increased, lands upslope were progressively brought into paddy cultivation. Thus, these hillside terraces, with increasing cultivation age from the top to the bottom of the slopes, provide soil chronosequences. A paddy soil chronosequence with paddy cultivation age of 0 year (P0), 60 years (P60), 150 years (P150), and 300 years (P300) was identified. Three typical soil profiles at each age were excavated. The history of paddy cultivation in the older profile at the bottom of the slope was determined from local historical literature from when the nearby villages were settled. For the newer profile at the top of the slope, information was obtained by questioning the local farmers. The uncultivated soil profile at the highest slope position was treated as the original soil, i.e., time zero with respect to paddy cultivation. The relative ages of the collected paddy soils were confirmed by Han (2012) using the profile development index (PDI) according to Harden (1982). Parent material homogeneity in the inter- and intra-profiles of the studied chronosequence (P0, P50, P150 and P300) was evaluated by making of using various soil attribute parameters (Han, 2012). Details of these profiles (P0, P60, P150, and P300) were given by Han and Zhang (2013), Han et al. (2015), and Huang et al. (2013, 2014, 2018), who investigated pedogenic changes in magnetic properties, clay minerals, and phosphorus fractions. The studied chronosequence is also a toposequence, which complicated the interpretation of the results (Zhang and Gong, 2003). In general, time of cultivation has the more significant role, since soil moisture regimes of paddy soils are maintained similarly. In hilly regions, terrace construction greatly reduces water loss and soil erosion and substantially weakens the influence of topography on pedogenesis. Additionally, all four sites are on geomorphically stable topographic positions with low slope gradient (< 5°), minimizing the effect of local erosion and deposition. Thus, the role of topography was not separately analyzed for different sampling sites, as we ascribed differential pedogenesis to the difference in time available for pedogenesis. Han and Zhang (2013) investigated changes in magnetism in three paddy soil chronosequences in the hilly regions of South China and showed that time of cultivation had a more significant role than the topography on the variations of magnetic properties.

2.2. Soil sampling and description

Within each area of identical paddy cultivation history, one representative profile was chosen for soil sampling based on soil landscape and geomorphological characteristics of that area. All soil samples were collected when the fields were drained after rice harvest. Soil profiles were described and sampled according to genetic horizons following standard field description guidelines (Schoeneberger et al., 2002; FAO, 2006). The uncultivated soil profile was generally homogeneous throughout its depth, with no observable horizon differentiation (Fig. 1). In contrast, the paddy soil profiles showed complicated patterns with depth due to anthropedogenesis and consisted of an anthrostagnic epipedon, including the cultivated horizon (Ap1) and the plow pan (Ap2), and a hydragric horizon (Bg) (Fig. 1). Differences in morphological properties, including soil color, texture and redoximorphic features, were also evident between the relatively younger pedon (60 years) and the older ones (150 and 300 years) (Fig. 1, and Table S1 in Supplementary material). Soils were defined as Udic Ferrosols (P0), Hapi-Stagnic Anthrosols (P60 and P150), and Fe-leachi-Stagnic Anthrosols (P300) by referring to Chinese Soil Taxonomy (Cooperative Research Group on Chinese Soil Taxonomy, 2001). The detailed field descriptions and classifications of the soil profiles are given in Table S1 in Supplementary material.

2.3. Analysis of basic soil physicochemical properties

After collection, samples of each soil horizon were dried at room temperature and then gently crushed using a wooden pestle and mortar and passed through a 2-mm nylon sieve. Soil bulk density was measured on the 100 cm^{-3} undisturbed soil cores by drying the cores for 24 h at 105 °C. The particle size distribution was determined by the pipette method and the clay content was defined as the mass percentage of particles < 2 μm in diameter for the whole soil. Soil pH was determined at a 1:2.5 soil/solution ratio using distilled water according to the Institute of Soil Science, Chinese Academy of Sciences (1978). Soil organic carbon (SOC) was measured by the Walkley-Black wet oxidation method (Nelson and Sommers, 1982) using the 149-μm fraction. Total nitrogen (N_{tot}) was measured by Kjeldahl method (Bremner, 1960) and total phosphorus (P_{tot}) was determined by $HClO_4$-HF digestion followed by colorimetric analysis (Institute of Soil Science, Chinese Academy of

Sciences, 1978). For total elemental analysis, soil samples (< 74 μm) were fused by a mixture of 1:1 lithium metaborate and lithium tetraborate for 30 min in a 1000 °C muffle furnace and then were dissolved in 10% HNO_3 + 1% HF solution. Total elemental concentrations including K, Na, Ca, Mg, Fe, Mn, Al, and Ti were determined by inductively coupled plasma-optical emission spectrometry. We estimate the precision as 5–10% relative standard deviation based on replicates and standard samples (Geochemical Standard Reference Sample Soil, GSS-3). The measured data are listed in Table S2 in Supplementary material. The dynamic changes in basic soil physicochemical properties have been reported by Han and Zhang (2013), Han et al. (2015), and Huang et al. (2013, 2014). Briefly, the studied chronosequence on a centennial time scale showed rapid accumulation of SOC and increase of pH in surface paddy soils, loss of clay and decrease of magnetic susceptibility with prolonged cultivation history, and shifts in phosphorus abundance and speciation as well as clay mineral compositions with both time and depth.

2.4. Extraction of Fe oxides and measurement of Fe concentrations

Bulk soil samples were subjected to reducing agents with increasing strength to selectively extract major pools of Fe: (1) the Tamm's extraction (Tamm, 1922); and (2) the citrate-bicarbonate-dithionite (CBD) extraction (Mehra and Jackson, 1960). The Tamm's extraction is a mixture of oxalic acid and ammonium oxalate, which was performed by shaking the sample-solution mixture in the dark over 4 h at 20 °C with a solid/liquid ratio of 1.25 g/50 ml. The Tamm's method targets the extraction of weakly bound, short-range-ordered (SRO) and organic bound Fe (Duchaufour and Souchier, 1966). For the extraction by CBD, soil samples were exposed to the reactant mixture at 80 °C for 30 min with a solid/liquid ratio of 0.5 g/25 ml. The CBD method extracts Fe in oxides and hydroxides (e.g., hematite, goethite, lepidocrocite) of all crystallinities—SRO and bulk crystalline (Mehra and Jackson, 1960). In addition to the partial extractions, total Fe was dissolved in a HF-$HClO_4$ mixture after calcination of soil organic matter at 450 °C. Fe concentrations in the extracted solutions were analyzed using an Inductively Coupled Plasma-Atomic Emission Spectrometer (ICP-AES, LAS Arras). We calculated the oxide bound Fe ($Fe_{oxide\text{-}bound}$) concentration by subtracting oxalate-extractable Fe (Fe_o) from the CBD-extractable Fe (Fe_d) ($Fe_{oxide\text{-}bound} = Fe_d - Fe_o$) and the silicate bound Fe ($Fe_{silicate\text{-}bound}$) was calculated by subtracting CBD-extractable Fe from the total Fe (Fe_t) concentration ($Fe_{oxide\text{-}bound} = Fe_t - Fe_d$).

2.5. Fe purification and Fe isotope measurements

An aliquot of powdered sample (< 74 μm, 100–500 mg depending on Fe content) was treated with 30% H_2O_2 to eliminate organic matter and then was dissolved completely in a microwave digestion with HF-HNO_3-HCl (1:1:3) for 30 min at 150 °C. Despite that organic matter was removed before digestion, samples with high organic matter in surface paddy soils were digested for 1 h in order to obtain a complete digestion. In addition, the digested clear solutions were evaporated in Teflon beakers on a hotplate and oxidized with HNO_3 and H_2O_2 to remove the potential remaining organic compounds and hydroxylamine and to convert Fe^{2+} to Fe^{3+}. The residue of this evaporation was re-dissolved in 6 M HCl for Fe separation and purification. Solution aliquots containing 100 μg Fe were purified using 1 ml of pre-cleaned anion exchange resin (Bio-Rad AG1 X4, 200–400 mesh) in 10 ml Bio-Rad polypropylene column (Bio-Rad #731-1550) in a metal-free clean chemistry laboratory following the procedure outlined in Wiederhold et al. (2007a, 2007b). Prior to purification, the anion exchange resin was cleaned according to Thompson et al. (2007). During the double chromatographic separation processes, Fe^{3+} was present as the $FeCl_4^-$ anion in 6 M HCl. The Fe complex was retained on the resin while the sample matrix was washed out by the repeated additions of 6 M HCl. Quantitative elution of Fe from the columns was achieved with 0.05 M HCl. The final eluted sample was evaporated to dryness with 1 drop of 30% H_2O_2 to ensure that all the Fe was in ferric form and then was re-dissolved in 0.3 M HNO_3. All the acids used during purification were cleaned in Teflon distills at sub-boiling conditions and prepared with ultrapure water (> 18 MX cm, Milli-Q, Millipore, USA). Recovery of Fe from the column after purification was found to be > 98% and the analytical blank was negligible (< 10 ng Fe) relative to the amounts of Fe (100 μg) loaded onto the columns.

Fe isotopic measurements were carried out at USTC (University of Science and Technology of China, Hefei) using a high-resolution multiple collector inductively coupled plasma mass spectrometer (MC-ICP-MS, Neptune Plus, Thermo Fisher Scientific) following the analytical procedure described by Schuth et al. (2015). Comprehensive descriptions of Fe isotope analytical methods were published by Schoenberg and von Blanckenburg (2005) and de Jong et al. (2007). Briefly, a standard-bracketing approach with IRMM-014 as standard reference material was used to correct for machine drift and instrumental mass bias (i.e., standard-sample-standard bracketing). The IRMM-014 solution and purified samples were adjusted to have the same Fe concentration of 0.3 mg l^{-1}. The sample solution was introduced into the plasma via a quartz glass double pass spray chamber combined with a PFA nebulizer. Interferences of $^{40}Ar^{14}N^+$, $^{40}Ar^{16}O^+$, and $^{40}Ar^{16}OH^+$ on the peaks of $^{54}Fe^+$, $^{56}Fe^+$ and $^{57}Fe^+$ were sufficiently resolved in medium resolution mode, thereby providing interference-free signal plateaus for Fe isotope measurements. Fe isotopic compositions from all samples were reported using standard delta notation in units of per mil (‰) relative to the standard reference material IRMM-014 using the following equation:

$$\delta^{56}Fe(‰) = \left[\frac{(^{56}Fe/^{54}Fe)sample}{(^{56}Fe/^{54}Fe)IRMM-014} - 1\right] \times 10^3 \quad (1)$$

Each sample and standard was measured at least four times and there was a replicate every ten samples. The precision of the isotopic compositions calculated on the basis of repeated measurements of the IRMM-014 standard was 0.04‰ (2SD) and 0.05‰ (2SD) for $\delta^{56}Fe$ and $\delta^{57}Fe$, respectively. The 2SD of $\delta^{56}Fe$ values of the soil samples with repeated measurements were < 0.06‰. In a $\delta^{57}Fe$ vs. $\delta^{57}Fe$ diagram, all soil sample and standard measurements plotted along a line with a slope of 1.471 (Fig. 2). This value is equal, within error margins, to the theoretical value of ln(M57/M6)/ln(M56/M54) = 1.487, indicating mass-dependent fraction and no influence of isobaric interferences.

2.6. Data analyses and calculations

Fe mass (kg m^{-2}) in the soil pedon was calculated by multiplying Fe concentrations by bulk density and thickness of soil horizons using the following equation:

$$Fe_{mass} = \sum_{i}^{n} C_{Fe} D_i E_i / 100 \quad (2)$$

where C_{Fe}, D_i, and E_i is, respectively, the Fe concentration (g kg^{-1}), bulk density (g cm^{-3}) and depth (cm) in the i horizon.

Loss and gain of Fe was computed by applying a simplified version of the open-system transport function (Brimhall and Dietrich, 1987; Chadwick et al., 1990), which ignored physical collapse and dilation of the soil column. The mass fraction of Fe lost or gained from a soil horizon relative to the mass of Fe originally present in the parent material was calculated using the following expression:

$$\tau_{Ti,Fe} = \frac{C_{Fe,w} C_{Ti,p}}{C_{Fe,p} C_{Ti,w}} - 1 \quad (3)$$

Here, C refers to the concentration (mg kg^{-1}) of immobile (Ti) and mobile (Fe) elements in the weathered (w) or parent (p) material. For the studied paddy soil chronosequence, Ti has been determined to be the least mobile element. Values of $\tau_{Ti,\ Fe} > 0$ indicate that Fe is

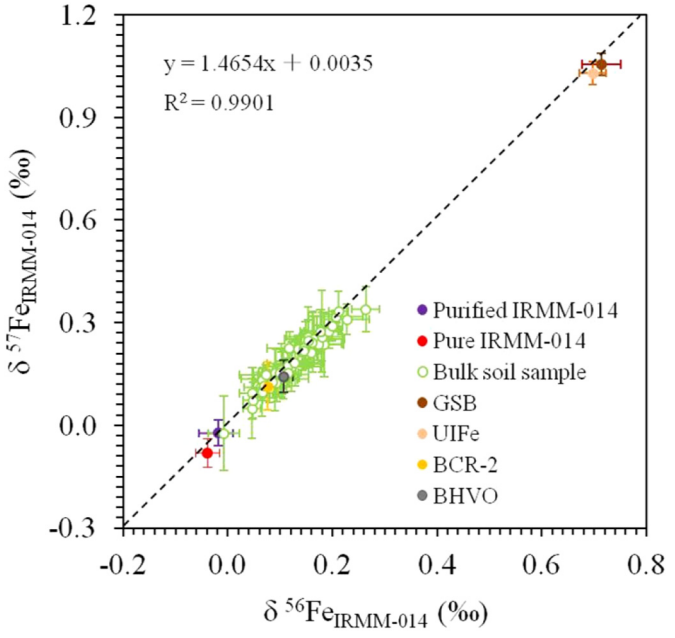

Fig. 2. $\delta^{57}Fe$ vs. $\delta^{56}Fe$ diagram of the data measured in this study. GSB: Fe standard in Institute of Geology and Geophysics, Chinese Academy of Sciences, recommended $\delta^{56}Fe_{IRMM\text{-}014} = 0.700 \pm 0.005‰$. UIFe: Fe standardand in University of Illinois, recommended $\delta^{56}Fe_{IRMM\text{-}014} = 0.695 \pm 0.005‰$; BCR-2: Basalt, Columbia River, Orgen, USA, recommended $\delta^{56}Fe_{IRMM\text{-}014} = 0.079 \pm 0.043‰$. BHVO: Basalt, Kilauea, Hawaii, USA, recommended $\delta^{56}Fe_{IRMM\text{-}014} = 0.105 \pm 0.008‰$. The diagonal line represents the theoretical mass-dependent fractionation between $\delta^{57}Fe$ and $\delta^{56}Fe$. Error bars are 2σ based on four replicates.

enriched in soil relative to parent material, while $\tau_{Ti,\ Fe} < 0$ indicates depletion and the absolute value of $\tau_{Ti,\ Fe}$ reveals the fraction of Fe left in soil relative to the parent material for the depleted samples.

Relationships between Fe concentrations and Fe isotopic ratios were analyzed by linear regression analysis, including regression diagnostics to ensure model appropriateness. Simple Pearson correlation coefficients among different soil properties were calculated. All statistical analyses were performed in the Statistical Package for the Social Sciences program (SPSS 13.0 for Windows, Chicago, IL, USA).

3. Results

3.1. Soil Fe content

Total Fe concentration and distribution was uniform throughout the soil profile in the uncultivated pedon (P0), ranging from 43.32 to 49.67 g kg^{-1} (Fig. 3). In contrast, the concentration and distribution of total Fe changed dramatically in paddy soils (P60, P150, and P300) as compared with that of uncultivated soil (P0) (Fig. 3), suggesting a transport and redistribution of Fe during anthropedogenesis. The standard deviation of total Fe concentration within 0–120 cm profile increased rapidly from 2.65 in the uncultivated pedon (P0) to 9.55 in the 60-year paddy soil (P60), and then decreased to 7.91 in the oldest paddy soil (P300). This variation occurred as total Fe declined more rapidly in the surface horizons as compared with that of the illuvial horizons in the 60- and 300-year paddy soils (P60 and P300). The 150-year paddy soil profile, however, showed relatively uniform distribution of total Fe, which we attributed to that the Fe input from the upslope may compensate the Fe loss by leaching in the surface horizon. The downward transport of Fe through the movement of fine particles has been reported along the hillslope of Susquehanna/Shale Hills Critical Zone Observatory (Jin et al., 2010). The weighted-mean total Fe concentration within 0–120 cm profile decreased gradually in the studied paddy soil chronosequence (P0, 44.45 g kg^{-1}; P60, 40.38 g kg^{-1}; P150, 35.68 g kg^{-1}; P300, 36.62 g kg^{-1}), suggesting a depletion of total Fe as paddy soils age. This was further confirmed by the negative values of $\tau_{Ti,\ Fe}$ in the studied paddy soil profiles (Table S3 in Supplementary material).

Selective extractions showed that the contributions of different Fe pools to total Fe varied along the soil depth and chronosequence (Fig. 3, and Table S3 in Supplementary material). The oxide bound Fe corresponded to 49–81% of the total Fe in the studied paddy soil chronosequence and its vertical distribution and evolution mimicked that of total Fe. This resulted in a strong correlation between the oxide bound Fe and total Fe, with a correlation coefficient of 0.92 ($n = 22$, $p < 0.01$) (Fig. 4). The weakly bound, poorly crystalline Fe pool corresponded to 4–18% of the total Fe and was present at consistently lower concentrations in the uncultivated soil as compared with that of paddy soils. The silicate bound Fe represented 11–40% of the total Fe and its concentration fluctuated with both soil depth and increasing paddy cultivation age.

3.2. Fe isotopic compositions

The $\delta^{56}Fe$ and its distribution was uniform (ranging from 0.10‰ to 0.12‰) throughout the soil profile in the uncultivated pedon (P0), corresponding to the relatively constant Fe concentrations (Fig. 5). This indicated virtually no vertical fractionation of Fe isotopes in the highly-weathered and Fe-rich Ferralsols (i.e., the uncultivated pedon P0). Li et al. (2017) also reported limited Fe isotope fractionation in the Ferralsols in the equatorial rainforest of Southern Philippines. In contrast, the amplitude of the Fe isotopic variations was much larger than the external reproducibility within the cultivated paddy soil profiles. The Fe isotopic compositions ($\delta^{56}Fe$) of the studied paddy soil chronosequence varied from 0.05‰ to 0.26‰ (Fig. 5), corresponding to the large fluctuations of Fe concentrations during paddy soil evolution. This suggests Fe isotope fractionation occurs during the centennial scale paddy soil evolution.

The $\delta^{56}Fe$ values in the surface horizons of 60- and 300-year paddy soils (P0, 0.19‰ and P300, 0.26‰) were higher than that of subsoils, indicating an enrichment of heavier Fe isotopes in the Fe-depleted horizons (Fig. 5). However, the 150-year paddy soil (P150) showed the highest $\delta^{56}Fe$ value (0.22‰) in the illuvial horizon (Br3, 35–48 cm) (Fig. 5). The lowest $\delta^{56}Fe$ value in the 60-, 150-, and 300-year paddy soil was respectively 0.05‰, 0.07‰ and 0.11%, which occurred at a much deeper horizon as paddy soils age (Fig. 5). The horizon near groundwater level in the 300-year paddy soil (P300) decreased in total Fe concentration but the $\delta^{56}Fe$ value was higher than the horizon immediate above (Fig. 5).

4. Discussions

4.1. Fe transfer, redistribution and depletion during upland paddy soil evolution

Fe is mobilized and translocated during paddy soil evolution as evidenced by the increasing differentiation of Fe mass and speciation within different selective extractions across the studied paddy soil chronosequence (Fig. 3). Previous studies have shown that rice cultivation results in coupled reduction-oxidation and eluviation-illuviation processes of Fe in paddy soils (Gong, 1983, 1986; Yu, 1985; Zhang and Gong, 1993, 2003; Han and Zhang, 2013) due to variations of soil pH and Eh induced by the artificial and seasonal water saturation and drainage (Kyuma, 2004). As a consequence, the formation of diagnostic horizons and features characterizing Fe distribution and redistribution in the vertical soil profiles occurs as paddy soils age (Fig. 1, and Table S1 in Supplementary material). In addition to the artificial submergence and drainage, seasonal fluctuations of groundwater level at the bottom of the slope also induce changes in soil redox potential

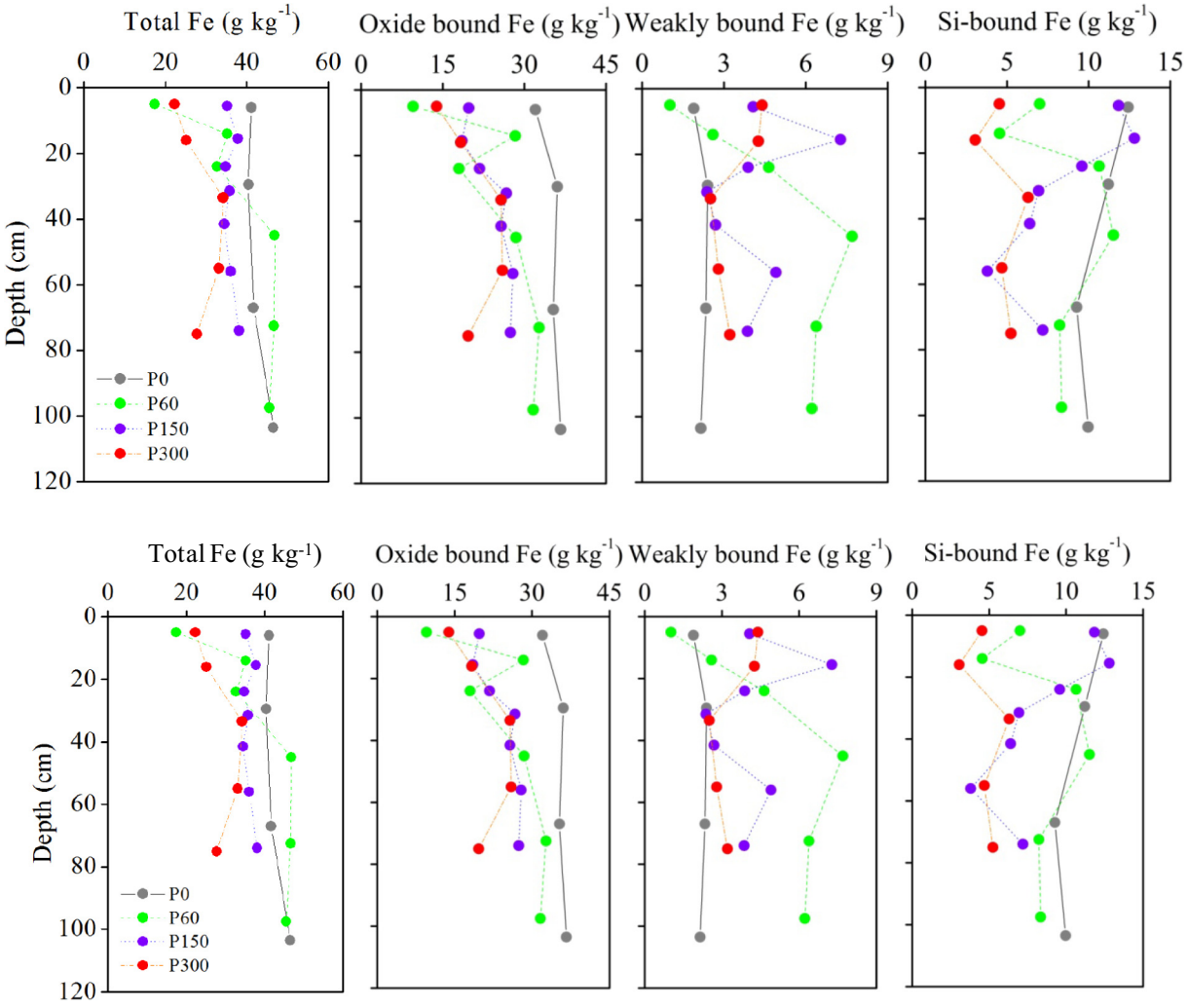

Fig. 3. Distributions and variations of total Fe, oxide bound Fe, weakly bound Fe, and silicate bound Fe concentrations along the soil depth and chronosequence.

(Ponnamperuma, 1972; Kirk, 2004). Huang et al. (2018a, 2018b) have demonstrated that the fluctuation of groundwater favors Fe reduction and depletion in the lower horizons of paddy soil profile in a plain area. This explains Fe depletion observed in the deeper layer of the 300-year paddy soil located at the bottom of the slope (Fig. 3).

Our results demonstrate that both artificial submergence and fluctuation of the groundwater level at the bottom of the slope are involved in the mobilization and translocation of Fe during paddy soil evolution. This results in changes in Fe fluxes and contributions of different Fe pools to total Fe within 0–120 cm soil layer (Fig. 7). Total Fe and oxide bound Fe decreased consistently from 73 and 59 kg m^{-2}, respectively, in the uncultivated soil to 42 and 31 kg m^{-2} after 300 years of rice cultivation. The average decreasing rate of total Fe (0.04 kg m^{-2} yr^{-1}) and oxide bound Fe (0.20 kg m^{-2} yr^{-1}) during the first 60 years of rice cultivation was, respectively, 0.36- and 2-fold of that between 60- and 300-year time period. The silicate bound Fe and weakly bound Fe increased initially from 11 and 3 kg m^{-2} in the uncultivated soil to 15 and 9 kg m^{-2} in the 60-year paddy soil, and then declined gradually to 7 and 4 kg m^{-2} in the 300-year paddy soil. Oxide bound Fe made up the largest proportion of total Fe across the studied paddy soil chronosequence. The contribution of oxide bound Fe to total Fe decreased initially (P0–P60) and then increased (P60–P300) as paddy soils age, while the proportion of weakly and silicate bound Fe to total Fe increased initially (P0–P60) and then decreased (P60–P300) with pedogenic time. Our results indicate the varying rates of Fe oxides changes during different stages of paddy soil evolution. Previous studies have shown that soil characteristics have different response times and associated thresholds during different stages of paddy soil evolution over a millennial time scale, which were attributed to changes in soil pH and redox potentials influenced by anthropogenic activities (Chen et al., 2011; Huang et al., 2018a, 2018b). In the upland regions, variations in leaching potentials have also been confirmed to affect the rates of Fe oxides transformations (Zhang and Gong, 2003).

The net depletion of Fe during paddy soil evolution over the centennial time scale, as confirmed by a combination of decreasing total Fe concentration (Fig. 3), the negative values of $\tau_{Ti,Fe}$ in paddy soils (Table S3 in Supplementary material) and the declined total Fe fluxes within 0–120 cm profile (Fig. 7), suggests Fe loss through leaching in solution as well as in colloids exceeds Fe input through artificial flooding and/or atmospheric deposition. Our results are consistent with the observation that rice cultivation over a decadal time scale could significantly enhance Fe depletion in the acid paddy soils developed on sloping upland areas (Zhang and Gong, 2003). Previous studies have shown that the critical redox potentials for Fe reduction and consequent dissolution are between +300 mV and + 100 mV at pH 6–7, and − 100 mV at pH 8,while at pH 5 appreciable Fe reduction occurred at +300 mV (Gotoh and Patrick, 1974). The pH value of our paddy soils derived from acid quaternary red clays ranged from 4.8 to 6.4 (Table S2 in Supplementary material). The acid environment together with the relatively high leaching potential in the sloping upland areas would promote Fe mobilization and leaching loss after artificial flooding (Fig. 4). This is confirmed by the rapid decrease of clay content in

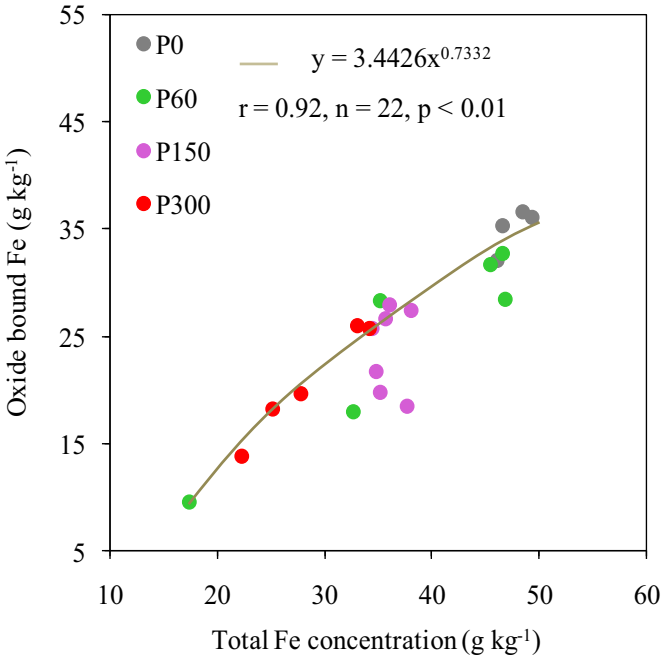

Fig. 4. Relationship between oxide bound Fe and total Fe in the studied paddy soil chronosequence.

paddy soils as compared with the original uncultivated soil (Table S2 in Supplementary material). Particle-facilitated leaching and transport of nutrients or metals have been extensively reported in the literature (e.g., de Jonge et al., 2004; Mohanty et al., 2014; Lu et al., 2016), which may partly explain the rapid decrease Fe of in acid paddy soils developed on the sloping upland areas.

4.2. Factors and processes controlling Fe isotope fractionation during upland paddy soil evolution

The uniform Fe isotopic composition with depth in the uncultivated Ferralsols (P0, Fig. 5) is consistent with the results reported by Poitrasson et al. (2008) and Li et al. (2017), indicating no vertical differentiation of Fe isotopic composition in Ferralsols before the establishment of paddy cultivation. This is attributed to that Fe remained mostly in oxidized form during Ferralsol evolution and thus resulted in little variation of the Fe isotope ratios in the vertical profiles (Poitrasson et al., 2008; Li et al., 2017). Fe isotopic composition of the paddy soil profiles becomes increasingly differentiated as a result of rice cultivation (Fig. 5). The $\Delta^{56}Fe_{profile}$ (i.e., the difference between the highest and lowest $\delta^{56}Fe$ values in a given soil profile) of P60, P150, and P300 (0.14–0.15) is greater than that of uncultivated pedon (P0, 0.02), suggesting a measurable Fe isotope fractionation occurs during the anthropedogenesis of paddy soils. Fe isotope fractionation in soils can be mediated by abiotic processes (proton-promoted or ligand-controlled Fe dissolution and mobilization, Fe adsorption and precipitation, and mineral transformation) as well as biotic processes (microbial reduction or oxidation of Fe) (Fantle and DePaolo, 2004; Emmanuel et al., 2005; Thompson et al., 2007; Wiederhold et al., 2007a, 2007b; Yamaguchi et al., 2007; Buss et al., 2010; Kiczka et al., 2011; Yesavage et al., 2012; Mansfeldt et al., 2012; Fekiacova et al., 2013; Akerman et al., 2014; Schuth et al., 2015; Garnier et al., 2017; Li et al., 2017). In paddy soils, the artificial periodic flooding and drainage are involved in the reduction-oxidation and eluviation-illuviation processes of Fe (Gong, 1983; Zhang and Gong, 2003). This results in the Fe translocation and redistribution within the vertical profile (Figs. 3 and 5). There is a strong negative correlation between $\delta^{56}Fe$ values and the logarithm of total Fe concentrations in the studied paddy soil chronosequence (Fig. 6), indicating the preferential loss of lighter Fe isotopes and thus enrichment of heavier Fe isotopes in the Fe-depleted horizons. This has been confirmed by relatively higher $\delta^{56}Fe$ values in the surface horizons and lower $\delta^{56}Fe$ values in the illuvial horizons of 60- and 300-year paddy soils (Fig. 5). In addition, the depth of the lowest $\delta^{56}Fe$ value in paddy soils increased with cultivation history (Fig. 5), suggesting lighter Fe isotopes are leaching into the deeper horizon as paddy soils age. However, given the large variations of Fe concentrations (Fig. 3), the mass-dependent Fe isotope fractionation effects in our paddy soils is relatively small compared with other redoximorphic soils (Wiederhold et al., 2007a). This suggests that other pedogenic processes could mask the Fe isotope effects induced by the reduction-oxidation and eluviation-illuviation processes of Fe in paddy soils.

4.3. Conceptual model of Fe dynamics during upland paddy soil evolution

We propose a conceptual model of Fe transfer and redistribution

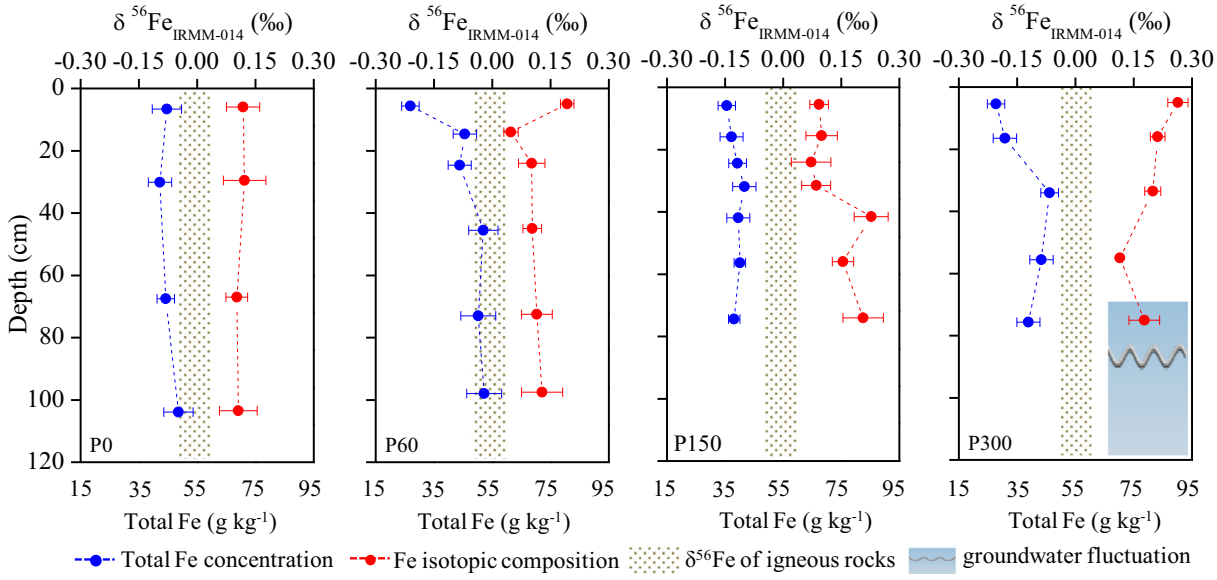

Fig. 5. Distributions and variations of the Fe isotopic compositions ($\delta^{56}Fe$) along the soil depth and chronosequence. Error bars represent 2 SD of replicate measurements.

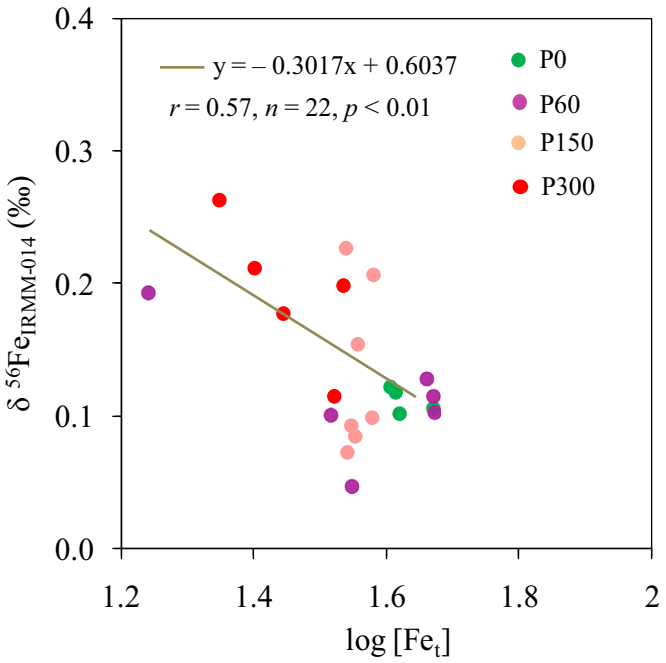

Fig. 6. Relationship between δ^{56}Fe values and total Fe concentrations in the studied paddy soil chronosequence.

during upland paddy soil evolution based on changing moisture regimes and redox conditions, and interpret their potential impacts on soil Fe isotope compositions (Fig. 8). As an open system, the studied paddy soils receive inputs of Fe from rice straw, which is expected to result in an enrichment of light Fe isotopes in the surface soil (①↓) (Fig. 8) because of the reported lighter Fe isotope compositions in rice plants (Garnier et al., 2017). In contrast, the δ^{56}Fe values of surface paddy soils (60- and 300-year) are greater than that of uncultivated soil (Fig. 5). This can be partly attributed to the rice uptake of Fe with lighter Fe isotopes, leaving the residual soils enriched in heavier Fe isotopes (②↑) as reported by Garnier et al. (2017). On the other hand, the reductive dissolution of Fe-bearing minerals and leaching of Fe both vertically (③↑) and horizontally (④↑) under reducing condition will cause an enrichment of heavier Fe isotopes in the surface horizon (Fig. 8). The decreased total Fe concentration and negative $\tau_{Ti,Fe}$ in the surface paddy soils (Table S3 in Supplementary material) suggest that Fe loss from topsoils through rice uptake, leaching in solution as well as in colloids (②, ③, ④) exceed Fe input through rice litter return. Schuth et al. (2015) have demonstrated that the net removal of Fe from the topsoil causes progressively higher soil δ^{56}Fe values due to the preferential release of ^{54}Fe. The vertical movement of low-δ^{56}Fe solution from the topsoil results with time in the formation of a subsoil with δ^{56}Fe values that are lower than the topsoil (60- and 300-year) (Fig. 5) after repeated low and high Eh cycles (③↓, Fig. 8). The heavier surface soil and lighter subsoil with respect to Fe isotopes have been confirmed by the δ^{56}Fe values of 60- and 300-year paddy soil profiles (Fig. 5). However, the δ^{56}Fe value in the surface soil of 150-year paddy profile is comparable to that of uncultivated soil (Fig. 5l), which we attributed to the leaching and transport of lighter Fe isotopes from the upper upslope to the lower slope (④↓). This happens due to the higher leaching potential in the upper slopes after conversion to paddy fields (Zhang and Gong, 2003). In the 300-year paddy profile, the groundwater fluctuation induced reductive dissolution and transport of Fe will result in an enrichment of heavier and lighter Fe isotopes in the horizon near groundwater level (⑤↑) and deeper horizons (⑤↓), respectively (Fig. 8). In addition, the lighter Fe isotopes can be leached out of the pedon (⑥↓) causing the enrichment of heavier Fe isotopes in the residual soil (⑥↑) (Fig. 8).

Therefore, the Fe isotope composition of a specific soil horizon is a result of a complex interaction of different processes in the upland paddy soils. It is currently difficult to evaluate the relative contribution of different processes to the Fe isotope fractionation during anthropedogenesis of upland paddy soils. Further investigations of Fe isotope signatures in the soil-plant-water system with a combination of laboratory simulation and prediction of Fe isotope fractionation for different processes as a result of paddy cultivation are needed to address this important question.

5. Conclusions

This study provides new insights into the behavior and geochemical cycle of Fe at the Earth's surface strongly affected by human activities and contributes to an improved understanding of how anthropedogenesis affects Fe evolution in the Earth's Critical Zone. Paddy soil development on QRC over a centennial time scale caused increasing profile differentiation of Fe oxides and measurable Fe isotope fractionation. Total Fe and oxide bound Fe as well as the maximum Fe illuviation depth decreased as paddy soils age, leading to significant differences in morphological properties between paddy and non-paddy soils developed on the same parent material. Selective extractions showed that the weakly-bound, oxide-bound and silicate bound Fe corresponded to 4–18%, 49–81%, and 11–40% of the total Fe, respectively, and these proportions varied with both time and depth due to the redox-related Fe transformation and redistribution. δ^{56}Fe values in the studied paddy soil chronosequence exhibited a strong negative correlation with the logarithm of total Fe concentrations, suggesting mass-dependent Fe isotope fractionation occurred as a result of the preferential removal of lighter Fe isotopes during Fe leaching loss under

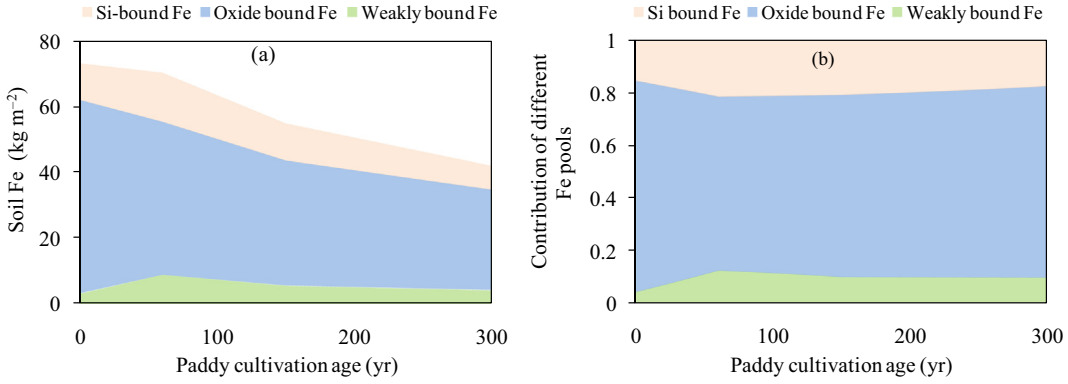

Fig. 7. Changes in Fe fluxes and the contributions of different Fe pools to total Fe within 0–120 cm soil layer during paddy soil development over the centennial time scale. Note: the assumed linear change in individual Fe pools in this study may not reflect the actual rates of change over the course of paddy soil development.

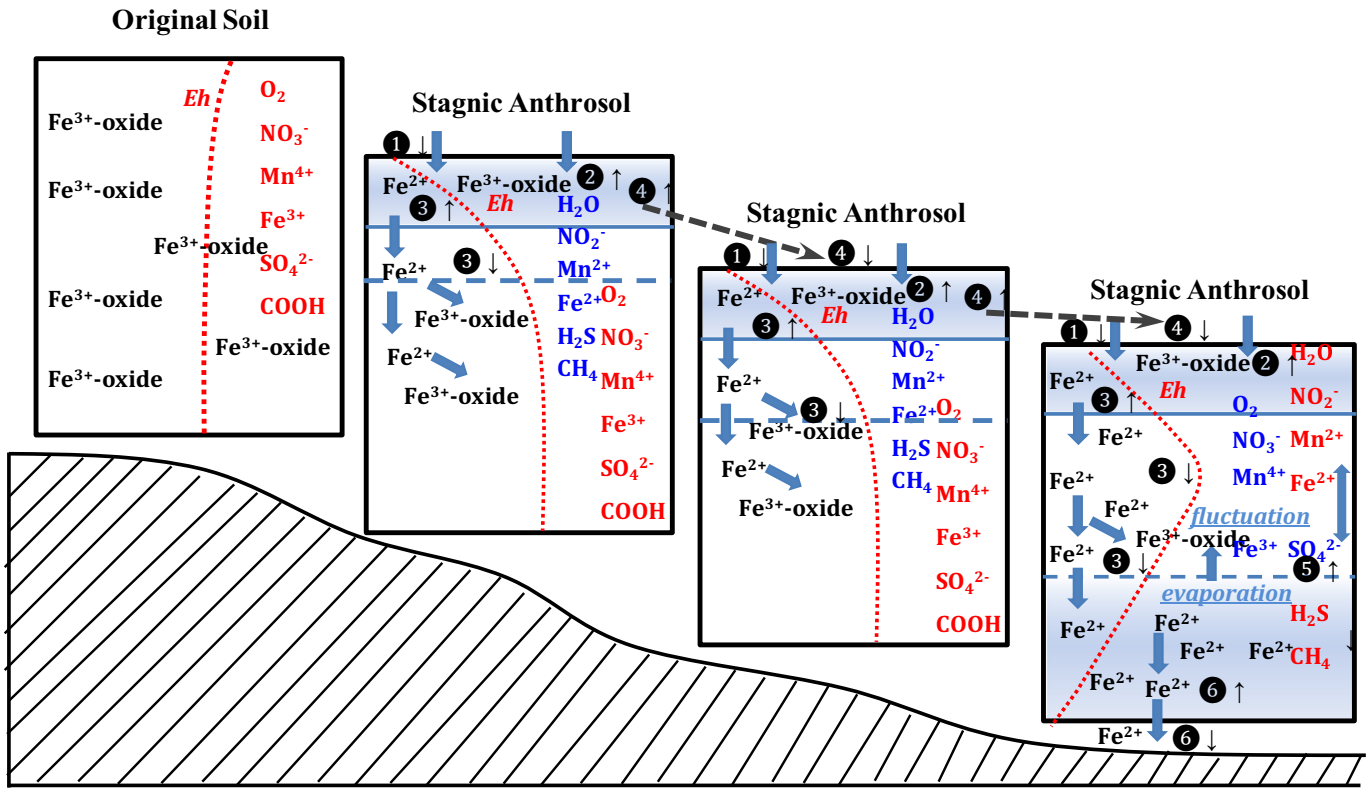

Fig. 8. Conceptual model of Fe transfer and redistribution processes in the upland paddy soil chronosequence and their potential impacts on Fe isotopic compositions in the soil profile with changing moisture regimes and redox conditions. ❶ External input of Fe with lighter Fe isotopes by rice straw return (↓); ❷ Rice uptake of Fe with lighter Fe isotopes, leading to the enrichment of heavier Fe isotopes in the cultivated horizon (↑); ❸ Reductive dissolution of Fe-bearing minerals in the cultivated horizon and transfer of lighter Fe isotopes to the illuvial horizons, causing the enrichment of heavier and lighter Fe isotopes in the cultivated (↑) and illuvial horizon (↓), respectively; ❹ Fe transport from the upper slopes to the lower slopes through leaching in solution and/or colloids, leading to the enrichment of heavier and lighter Fe isotopes in the surface horizons of the upper slopes (↑) and lower slopes (↓), respectively. ❺ Groundwater fluctuation induced reductive dissolution of Fe-bearing minerals and transport of lighter Fe isotopes to the lower horizons, resulting in the enrichment of heavier and lighter Fe isotopes in the horizon near groundwater level (↑) and deeper horizons (↓), respectively; ❻ Lighter Fe isotopes leaching out of pedon, causing the enrichment of heavier Fe isotopes in the residual soil (↑).

the predominant reducing conditions. However, the Fe isotopic ratio of a specific paddy soil horizon was a result of a complex interaction of different processes, which were summarized and interpreted in our proposed conceptual model of Fe evolution. Further investigations of Fe isotope signatures in the soil-plant-water system with a combination of laboratory simulation and prediction of Fe isotope fractionation under different pedogenic processes are needed to evaluate the relative contribution of multiple processes to Fe isotope fractionation during the anthropedogenesis of paddy soils.

Acknowledgements

We are grateful to Decheng Li, Institute of Soil Science, Chinese Academy of Sciences, and Hong Lu, Cixi Agriculture Bureau, Zhejiang Province, for their help during the field work. We also thank Alan Matthews, Ami Nishri, Jan Wiederhold, Nadya Teutsch, Stephan Kraemer, and Yigal Erel for their patient training on Fe column chemistry and Fe isotope measurements during FIMIN workshop held at The Hebrew University of Jerusalem, Israel. This study was supported by projects from the Natural Science Foundation of China (Grant no. 41601221 and 41571130051), Ministry of Science and Technology of China (Grant no. 2016YFC0501605), Outstanding Young Talent Project from Institute of Geographic Sciences and Natural Resources Research (Grant no. 2017RC203), State Key Laboratory of Soil and Sustainable Agriculture, Institute of Soil Science, Chinese Academy of Sciences (Grant no. Y20160003), State Key Laboratory of Soil Erosion and Dryland Farming on the Loess Plateau, Institute of Soil and Water Conservation, Chinese Academy of Sciences (Grant no. A314021402-1602), and Key Laboratory of Ecosystem Network Observation and Modeling, Institute of Geographic Sciences and Natural Resources Research, Chinese Academy of Sciences (Grant no. LENOM2016Q0001).

References

Akerman, A., Poitrasson, F., Oliva, P., Audry, S., Prunier, J., Braun, J.J., 2014. The isotopic fingerprint of Fe cycling in an equatorial soil–plant–water system: the Nsimi watershed, South Cameroon. Chem. Geol. 385, 104–116.
Anbar, A.D., 2004. Iron stable isotopes: beyond biosignatures. Earth Planet. Sci. Lett. 217, 223–236.
Anbar, A.D., Roe, J.E., Barling, J., Nealson, K.H., 2000. Nonbiological fractionation of iron isotopes. Science 288, 126.
Aniku, J.R.F., Singer, M.J., 1990. Pedogenic iron oxide trends in a marine terrace chronosequence. Soil Sci. Soc. Am. J. 54, 147–152.
Balci, N., Bullen, T.D., Witte-Lien, K., Shanks, W.C., Motelica, M., Mandernack, K.W., 2006. Iron isotope fractionation during microbially stimulated Fe(II) oxidation and Fe(III) precipitation. Geochim. Cosmochim. Acta 70, 622–639.
Beard, B.L., Johnson, C.M., Cox, L., Sun, H., Nealson, K.H., Aguilar, C., 1999. Iron isotope biosignatures. Science 285, 1889.
Brantley, S.L., Liermann, L., Bullen, T.D., 2001. Fractionation of Fe isotopes by soil microbes and organic acids. Geology 29, 535–538.
Brantley, S.L., Liermann, L.J., Guynn, R.L., Anbar, A., Icopini, G.A., Barling, J., 2004. Fe isotopic fractionation during mineral dissolution with and without bacteria1. Geochim. Cosmochim. Acta 68, 3189–3204.
van Breemen, N., Buurman, P., 2004. Soil Formation, 2nd ed. Kluwer Acad. Publ., Dordrecht, the Netherlands.
Bremner, J.M., 1960. Determination of nitrogen in soil by the Kjeldahl method. J. Agric. Sci. 55, 11–33.
Brimhall, G.H., Dietrich, W.E., 1987. Constitutive mass balance relations between

chemical composition, volume, density, porosity, and strain in metasomatic hydrochemical systems: results on weathering and pedogenesis. Geochim. Cosmochim. Acta 51, 567–587.
Buss, H.L., Mathur, R., White, A.F., Brantley, S.L., 2010. Phosphorus and iron cycling in deep saprolite, Luquillo Mountains, Puerto Rico. Chem. Geol. 269, 52–61.
Chadwick, O.A., Brimhall, G.H., Hendricks, D.M., 1990. From a black to a gray box—a mass balance interpretation of pedogenesis. Geomorphology 3, 369–390.
Chen, L.M., Zhang, G.L., Effland, W.R., 2011. Soil characteristic response times and pedogenic thresholds during the 1000-year evolution of a paddy soil chronosequence. Soil Sci. Soc. Am. J. 75, 1807–1820.
Chen, L.M., Zhang, G.L., Rossiter, D.G., Cao, Z.H., 2015. Magnetic depletion and enhancement in the evolution of paddy and non-paddy soil chronosequences. Eur. J. Soil Sci. 66, 886–897.
Cooperative Research Group on Chinese Soil Taxonomy, 2001. Chinese Soil Taxonomy. Science Press, Beijing (in Chinese).
Cornell, R.M., Schwertmann, U., 2003. The Iron Oxides: Structure, Properties, Reactions, Occurrences, and Uses. Wiley-VCH Verlag GmbH & Co. KGaA, Weinheim.
Crosby, H.A., Johnson, C.M., Roden, E.E., Beard, B.L., 2005. Coupled Fe (II)-Fe (III) electron and atom exchange as a mechanism for Fe isotope fractionation during dissimilatory iron oxide reduction. Environ. Sci. Technol. 39, 6698–6704.
Crosby, H.A., Roden, E.E., Johnson, C.M., Beard, B.L., 2007. The mechanisms of iron isotope fractionation produced during dissimilatory Fe (III) reduction by *Shewanella putrefaciens* and *Geobacter sulfurreducens*. Geobiology 5, 169–189.
Dauphas, N., Rouxel, O., 2006. Mass spectrometry and natural variations of iron isotopes. Mass Spectrom. Rev. 25, 515–550.
Dauphas, N., John, S.G., Rouxel, O., 2017. Iron isotope systematic. Rev. Mineral. Geochem. 82, 415–510.
Duchaufour, P., Souchier, B., 1966. Note sur une méthode d'extraction combinée de l'aluminium et du fer libres dans les sols. Science du sol 1, 17–29.
Dudal, R., 2005. The sixth factor of soil formation. Eurasian Soil Sci. 38, S60.
Emmanuel, S., Erel, Y., Matthews, A., Teutsch, N., 2005. A preliminary mixing model for Fe isotopes in soils. Chem. Geol. 222, 23–34.
Fantle, M.S., DePaolo, D.J., 2004. Iron isotopic fractionation during continental weathering. Earth Planet. Sci. Lett. 228, 547–562.
FAO, 2006. World Reference Base for Soil Resources. World Soil Resour. Rep. 103 FAO, Rome.
Fekiacova, Z., Pichat, S., Cornu, S., Balesdent, J., 2013. Inferences from the vertical distribution of Fe isotopic compositions on pedogenetic processes in soils. Geoderma 209, 110–118.
Garnier, J., Garnier, J.M., Vieira, C.L., Akerman, A., Chmeleff, J., Ruiz, R.I., Poitrasson, F., 2017. Iron isotope fingerprints of redox and biogeochemical cycling in the soil-water-rice plant system of a paddy field. Sci. Total Environ. 574, 1622–1632.
Gong, Z.T., 1983. Pedogenesis of paddy soils and its significance in soil classification. Soil Sci. 35, 5–10.
Gong, Z.T., 1985. In: Li, Q.K. (Ed.), Bio-geochemistry of the Red Weathering Crusts. Red Soils in China Science Press, Beijing, pp. 24–40 (in Chinese).
Gong, Z.T., 1986. Origin, evolution and classification of paddy soils in China. Adv. Soil Sci. 5, 174–200.
Gotoh, S., Patrick, W.H., 1974. Transformation of iron in a waterlogged soil as influenced by redox potential and pH. Soil Sci. Soc. Am. J. 38, 66–71.
Han, G.Z., 2012. Pedogenesis of Hydragric Anthrosols Chronosequences From Different Parent Materials in South China. Doctoral Dissertation. Institute of Soil Science, Chinese Academy of Soil Sciences (in Chinese).
Han, G.Z., Zhang, G.L., 2013. Changes in magnetic properties and their pedogenetic implications for paddy soil chronosequences from different parent materials in south China. Eur. J. Soil Sci. 64, 435–444.
Han, G.Z., Zhang, G.L., Li, D.C., Yang, J.L., 2015. Pedogenetic evolution of clay minerals and agricultural implications in three paddy soil chronosequences of south China derived from different parent materials. J. Soils Sediments 15, 423–435.
Harden, J.W., 1982. A quantitative index of soil development from field descriptions: examples from a soil chronosequence in central California. Geoderma 28, 1–28.
He, Y., Li, D.C., Velde, B., Yang, Y.F., Huang, C.M., Gong, Z.T., Zhang, G.L., 2008. Clay minerals in a soil chronosequence derived from basalt on Hainan Island, China and its implication for pedogenesis. Geoderma 148, 206–212.
Hong, H., Churchman, G.J., Yin, K., Li, R.B., Li, Z.H., 2014. Randomly interstratified illite–vermiculite from weathering of illite in red earth sediments in Xuancheng, southeastern China. Geoderma 214, 42–49.
Hu, X.F., Wei, J., Du, Y., Xu, L.F., Wang, H.B., Zhang, G.L., Ye, W., Zhu, L.D., 2010. Regional distribution of the Quaternary Red Clay with aeolian dust characteristics in subtropical China and its paleoclimatic implications. Geoderma 159, 317–334.
Huang, L.M., Zhang, G.L., Thompson, A., Rossiter, D.G., 2013. Pedogenic transformation of phosphorus during paddy soil development on calcareous and acid parent materials. Soil Sci. Soc. Am. J. 77, 2078–2088.
Huang, L.M., Thompson, A., Zhang, G.L., 2014. Long-term paddy cultivation significantly alters topsoil phosphorus transformation and degrades phosphorus sorption capacity. Soil Tillage Res. 142, 32–41.
Huang, L.M., Thompson, A., Zhang, G.L., Chen, L.M., Han, G.Z., Gong, Z.T., 2015. The use of chronosequences in studies of paddy soil evolution: a review. Geoderma 237, 199–210.
Huang, L.M., Jia, X.X., Shao, M.A., Chen, L.M., Han, G.Z., Zhang, G.L., 2018a. Phases and rates of iron and magnetism changes during paddy soil development on calcareous marine sediment and acid Quaternary red-clay. Sci. Rep. http://dx.doi.org/10.1038/s41598-017-18963-x.
Huang, L.M., Jia, X.X., Zhang, G.L., Thompson, A., Huang, F., Shao, M.A., Chen, L.M., 2018b. Variations and controls of iron oxides and isotope compositions during paddy soil evolution over a millennial time scale. Chem. Geol. 476, 340–351.
Icopini, G.A., Anbar, A.D., Ruebush, S.S., Tien, M., Brantley, S.L., 2004. Iron isotope fractionation during microbial reduction of iron: the importance of adsorption. Geology 32, 205–208.
Institute of Soil Science, Chinese Academy of Sciences, 1978. Methods for Soil Physical and Chemical Analysis. Shanghai Sci. and Technol. Press, Shanghai (in Chinese).
Jin, L.X., Ravella, R., Ketchum, B., Bieman, P.R., Heaney, P., White, T., Brantley, S.L., 2010. Mineral weathering and elemental transport during hillslope evolution at the Susquehanna/Shale Hills Critical Zone Observatory. Geochim. Cosmochim. Acta 74, 3669–3691.
Johnson, C.M., Beard, B.L., Roden, E.E., Newman, D.K., Nealson, K.H., 2004. Isotopic constraints on biogeochemical cycling of Fe. Rev. Mineral. Geochem. 55 (359–40).
de Jong, J., Schoemann, V., Tison, J.L., Becquevort, S., Masson, F., Lannuzel, D., Petit, J., Chou, L., Weis, D., Mattielli, N., 2007. Precise measurement of Fe isotopes in marine samples by multi-collector inductively coupled plasma mass spectrometry (MC-ICP-MS). Anal. Chim. Acta 589, 105–119.
de Jonge, L.W., Moldrup, P., Rubæk, G.H., Schelde, K., Djurhuus, J., 2004. Particle leaching and particle-facilitated transport of phosphorus at field scale. Vadose Zone J. 3, 462–470.
Kappler, A., Johnson, C.M., Crosby, H.A., Beard, B.L., Newman, D.K., 2010. Evidence for equilibrium iron isotope fractionation by nitrate-reducing iron (II)-oxidizing bacteria. Geochim. Cosmochim. Acta 74, 2826–2842.
Kiczka, M., Wiederhold, J.G., Frommer, J., Voegelin, A., Kraemer, S.M., Bourdon, B., Kretzschmar, R., 2011. Iron speciation and isotope fractionation during silicate weathering and soil formation in an alpine glacier forefield chronosequence. Geochim. Cosmochim. Acta 75, 5559–5573.
Kirk, G., 2004. The Biogeochemistry of Submerged Soils. John Wiley & Sons, Chichester, UK.
Kyuma, K., 2004. Paddy Soil Science. Kyoto University Press, Kyoto, Japan.
Li, Q.K., 1983. Red Soils in China. Science Press, Beijing (in Chinese).
Li, Q.K., 1992. Paddy Soils in China. Science Press, Beijing (in Chinese).
Li, M., He, Y.S., Kang, J.T., Yang, X.Y., He, Z.W., Yu, H.M., Huang, F., 2017. Why was iron lost without significant isotope fractionation during the lateritic process in tropical environments? Geoderma 290, 1–9.
Lu, C., Wu, Y., Hu, S., 2016. Drying–wetting cycles facilitated mobilization and transport of metal-rich colloidal particles from exposed mine tailing into soil in a gold mining region along the Silk Road. Environ. Earth Sci. 75, 1–12.
Mansfeldt, T., Schuth, S., Häusler, W., Wagner, F.E., Kaufhold, S., Overesch, M., 2012. Iron oxide mineralogy and stable iron isotope composition in a Gleysol with petrogleyic properties. J. Soils Sediments 12, 97–114.
Matthews, A., Zhu, X.K., O'Nions, K., 2001. Kinetic iron stable isotope fractionation between iron (-II) and (-III) complexes in solution. Earth Planet. Sci. Lett. 192, 81–92.
Mehra, O.P., Jackson, M.L., 1960. Iron oxide removal from soils and clays by a dithionite-citrate system buffered with sodium bicarbonate. Clay Clay Miner. 7, 317–327.
Mohanty, S.K., Saiers, J.E., Ryan, J.N., 2014. Colloid-facilitated mobilization of metals by freeze–thaw cycles. Environ. Sci. Technol. 48, 977–984.
Muggler, C.C., Van Loef, J.J., Buurman, P., van Doesburg, J.D.J., 2001. Mineralogical and (sub)microscopic aspects of iron oxides in polygenetic Oxisols from Minas Gerais, Brazil. Geoderma 100, 147–171.
Nelson, D.W., Sommers, L.E., 1982. Total carbon, organic carbon and organic matter. In: Page, A.L., Miller, R.H., Keeney, D.R. (Eds.), Methods of Soil Analysis. Part 2, 2nd ed. Agron. Monogr. 9 ASA and SSSA, Madison, WI, pp. 539–577.
Poitrasson, F., Viers, J., Martin, F., Braun, J.J., 2008. Limited iron isotope variations in recent lateritic soils from Nsimi, Cameroon: implications for the global Fe geochemical cycle. Chem. Geol. 253, 54–63.
Ponnamperuma, F.N., 1972. The chemistry of submerged soils. Adv. Agron. 24, 29–96.
Schoenberg, R., von Blanckenburg, F., 2005. An assessment of the accuracy of stable Fe isotope ratio measurements on samples with organic and inorganic matrices by high-resolution multicollector ICP-MS. Int. J. Mass Spectrom. 242, 257–272.
Schoeneberger, P.J., Wysocki, D.A., Benham, E.C., Broderson, W.D., 2002. Field Book for Describing and Sampling Soils, 2nd ed. Natl. Soil Surv. Ctr., Lincoln, NE.
Schuth, S., Hurraß, J., Münker, C., Mansfeldt, T., 2015. Redox-dependent fractionation of iron isotopes in suspensions of a groundwater-influenced soil. Chem. Geol. 392, 74–86.
Skulan, J., Beard, B., Johnson, C., 2002. Kinetic and equilibrium Fe isotope fractionation between aqueous Fe(III) and hematite. Geochim. Cosmochim. Acta 66, 2995–3015.
Tamm, O., 1922. Eine method zur bestimmung der anorganishen komponenten des golkomplex im boden. Medd. Statens Skogforsoksanst 19, 385–404.
Thompson, A., Ruiz, J., Chadwick, O.A., Titus, M., Chorover, J., 2007. Rayleigh fractionation of iron isotopes during pedogenesis along a climate sequence of Hawaiian basalt. Chem. Geol. 238, 72–83.
Torrent, J., Schwertmann, U., Schulze, D.G., 1980. Iron oxide mineralogy of some soils of two river terrace sequences in Spain. Geoderma 23, 191–208.
Vodyanitskii, Y.N., 2010. Iron hydroxides in soils: a review of publications. Eurasian Soil Sci. 43, 1244–1254.
Wiederhold, J.G., Kraemer, S.M., Teutsch, N., Borer, P.M., Halliday, A.N., Kretzschmar, R., 2006. Iron isotope fractionation during proton-promoted, ligand-controlled, and reductive dissolution of goethite. Environ. Sci. Technol. 40, 3787–3793.
Wiederhold, J.G., Teutsch, N., Kraemer, S.M., Halliday, A.N., Kretzschmar, R., 2007a. Iron isotope fractionation during pedogenesis in redoximorphic soils. Soil Sci. Soc. Am. J. 71, 1840–1850.
Wiederhold, J.G., Teutsch, N., Kraemer, S.M., Halliday, A.N., Kretzschmar, R., 2007b. Iron isotope fractionation in oxic soils by mineral weathering and podzolization. Geochim. Cosmochim. Acta 71, 5821–5833.
Yamaguchi, K.E., Johnson, C.M., Beard, B.L., Beukes, N.J., Gutzmer, J., Ohmoto, H., 2007. Isotopic evidence for iron mobilization during Paleoproterozoic lateritization of the Hekpoort paleosol profile from Gaborone, Botswana. Earth Planet. Sci. Lett.

256, 577–587.
Yesavage, T., Fantle, M.S., Vervoort, J., Mathur, R., Jin, L., Liermann, L.J., Brantley, S.L., 2012. Fe cycling in the Shale Hills Critical Zone Observatory, Pennsylvania: an analysis of biogeochemical weathering and Fe isotope fractionation. Geochim. Cosmochim. Acta 99, 18–38.
Yu, T.R., 1985. Physical Chemistry of Paddy Soils. Science Press, Beijing, China.
Zhang, G.L., Gong, Z.T., 1993. Geochemical features of element migration under artificial submergence. Acta Pedol. Sin. 30, 355–365 (in Chinese).
Zhang, G.L., Gong, Z.T., 2003. Pedogenic evolution of paddy soils in different soil landscapes. Geoderma 115, 15–29.